Mechanistic insights into the formation of N-vacancies at sp^2 hybridized sites in non-metal doped g-C_3N_4 and its potential applications in Solar to H_2 conversion and environmental remediation reactions

Rama Krishna Chava,*[a] Annamalai Raja,[a] Sathish Panner Selvam,[b] Shanmugasundaram Kamalakannan,[c] and Misook Kang*[a]

[a]Department of Chemistry, College of Natural Sciences, Yeungnam University, 280 Daehak-Ro, Gyeongsan, Gyeongbuk 38541, Republic of Korea

[b]Department of Electronic Engineering, Gachon University, Seongnam-si, Gyeonggi-do 13210, Republic of Korea

[c]Centre of Excellence in Materials and Advanced Technologies (CeMAT), Faculty of Engineering and Technology, SRM Institute of Science and Technology, Kattankulathur, 603203, Chennai, Tamil Nadu, India

Corresponding authors address:

Dr. Rama Krishna Chava: Department of Chemistry, College of Natural Sciences, Yeungnam University, 280 Daehak-Ro, Gyeongsan, Gyeongbuk 38541, Republic of Korea.

Email: drcrkphysics@hotmail.com; rama@ynu.ac.kr

Prof. Misook Kang: Department of Chemistry, College of Natural Sciences, Yeungnam University, 280 Daehak-Ro, Gyeongsan, Gyeongbuk 38541, Republic of Korea.

Email: mskang@ynu.ac.kr

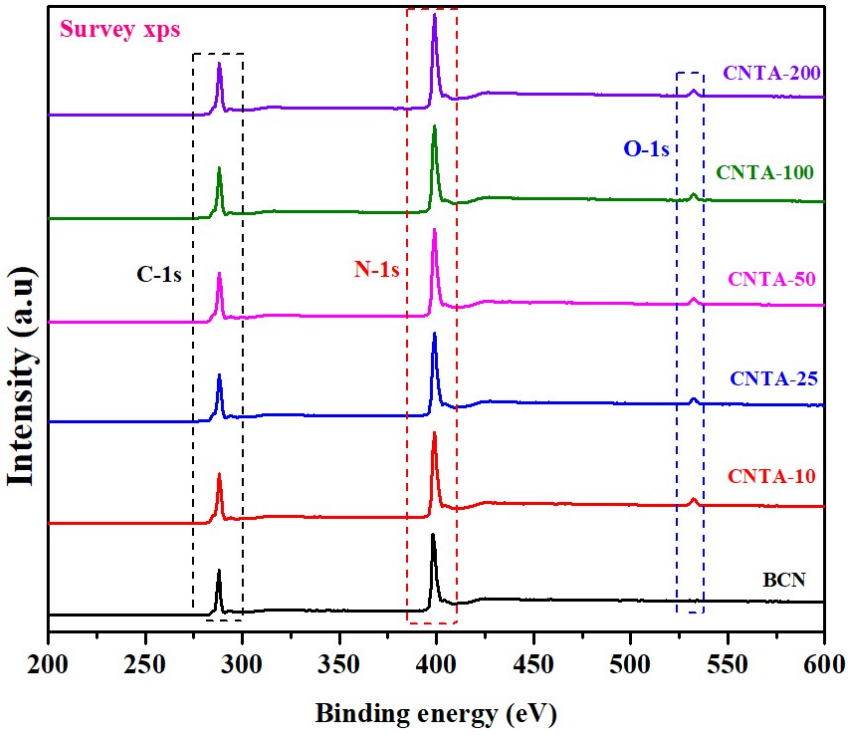

Fig. S1. XPS survey scan spectra of BCN and CNTA samples.

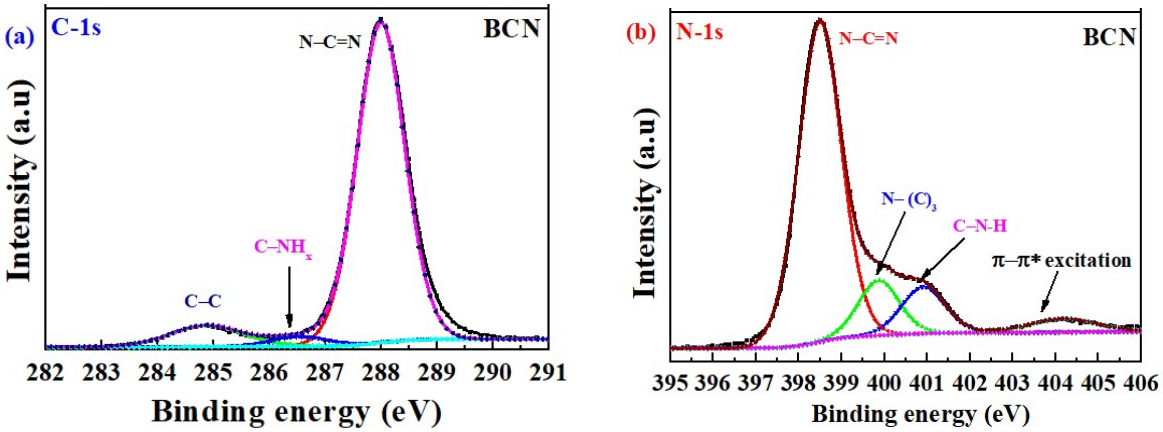

Fig. S2. High-resolution XPS spectra of BCN sample (a) C-1s displayed peaks around 284.85, 286.40 and 288.00 eV attributed to graphitic carbon in C–C or C=C sites, C–NHx (x=1 or 2), N–C=N in the aromatic rings of the g-C_3N_4 heterocycles respectively; and (b) N-1s exhibited the peaks at 398.50, 399.85, 400.95 and 404.25 eV corresponds to sp^2-hybridized nitrogen in triazine rings, N–$(C)_3$, sp^3 primary nitrogen atom (N–H/NH_2) and charge localization effect respectively.

Table S1. Relative atomic percentage details of C-1s, N-1s and O-1s elements in BCN and CNTA samples

Sample	C-1s (at %)	N-1s (at %)	O-1s (at %)	N/C	C/N
BCN	40.65	59.35	-	1.460	0.685
CNTA-10	42.50	54.25	3.25	1.276	0.783
CNTA-25	42.60	54.37	3.03	1.276	0.783
CNTA-50	42.47	54.55	2.99	1.284	0.778
CNTA-100	42.22	54.81	2.97	1.298	0.770
CNTA-200	41.97	55.27	2.77	1.317	0.759

Table S2. The ratio of peak areas for BCN and CNTA-100 based on XPS N-1s results.

Sample	N-1s (at %)		
	C=N–C	$N–(C)_3$	C–NHx
BCN	63.8%	27.4%	8.8%
CNTA-100	48.5%	35.7%	15.8%

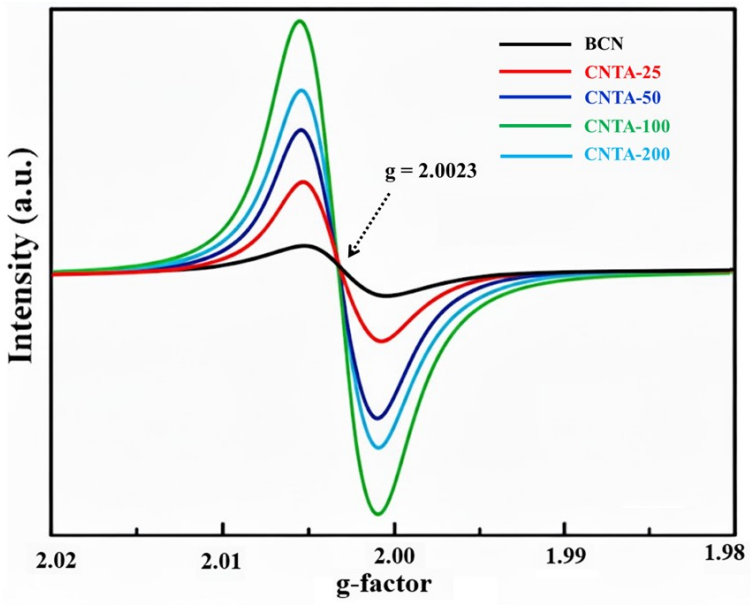

Fig. S3. DPPH calibrated electron paramagnetic resonance (EPR) spectra of BCN and CNTA samples.

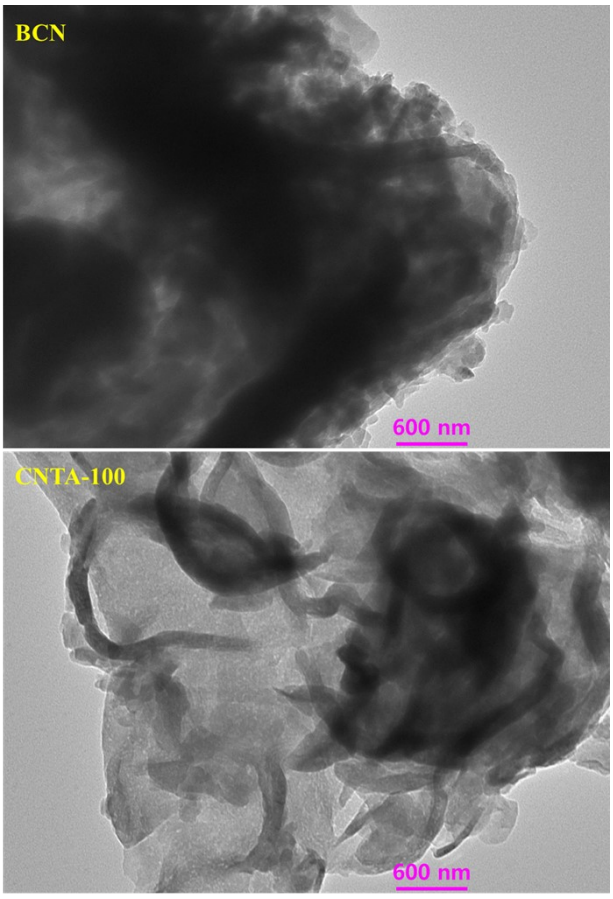

Fig. S4. High magnification TEM images of BCN and CNTA-100 photocatalyst samples to highlight the formation of pores on the surface of g-C_3N_4.

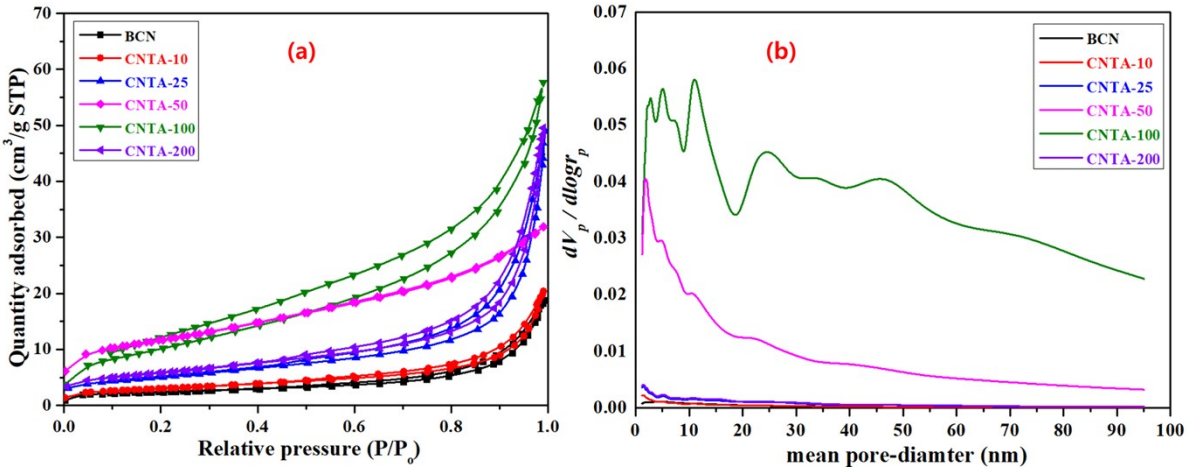

Fig. S5. N_2 adsorption-desorption isotherms (a) and pore-size distribution curves (b) of BCN and CNTA samples.

Table S3. BET surface area and pore-size distribution parameters for BCN and CNTA samples

Sample	**BET surface area (m^2/g)**	**mean pore diameter (nm)**	**pore volume (cm^3/g)**
BCN	10.41	4.92	0.012
CNTA-10	10.51	4.93	0.013
CNTA-25	17.63	15.50	0.068
CNTA-50	19.98	15.10	0.075
CNTA-100	23.80	15.17	0.075
CNTA-200	17.86	4.96	0.022

Table S4. Comparison of photocatalytic H_2 evolution activity of the CNTA-100 sample with the recent non-metal doped and defects engineered g-C_3N_4 photocatalysts.

Catalyst	**Light source**	**H_2 evolution rate ($\mu mol.g^{-1}.h^{-1}$)**	**Apparent Quantum Yield (AQY%)**	**Ref.**
C, O- doped g-C_3N_4	300 W Xe lamp 200-2500 nm	563.87	---	[1]
S-doped g-C_3N_4	300 W Xe lamp ($\lambda \geq 420$ nm)	133.12	---	[2]
g-C_3N_4 with N_v	300 W Xe lamp ($\lambda \geq 420$ nm)	2664.47	9.8%	[3]
C and O- co-doped g-C_3N_4	300 W Xe lamp ($\lambda \geq 420$ nm)	2595.4	16.6%	[4]
N-defected g-C_3N_4	300 W Xe lamp ($\lambda \geq 400$ nm)	316.0	5.12%	[5]
g-C_3N_4 with N_{3C} vacancies	300 W Xe lamp ($\lambda \geq 420$ nm)	545.0	4.4%	[6]
P-doped g-C_3N_4	300 W Xe lamp ($\lambda \geq 420$ nm)	916.2	6.52%	[7]
hollow tubular g-C_3N_4 with N_v	300 W Xe lamp ($\lambda \geq 420$ nm)	2664.4	9.8%	[8]
S-doped N-deficient g-C_3N_4	300 W Xe lamp ($\lambda \geq 420$ nm)	1613.5	14.3%	[9]
S-doped C-vacancy g-C_3N_4	300 W Xe lamp ($\lambda \geq 420$ nm)	2378	5.70%	[10]
Dual defect-rich g-C_3N_4	300 W Xe lamp ($\lambda \geq 420$ nm)	1959	0.21%	[11]
N-deficient g-C_3N_4	300 W Xe lamp ($\lambda \geq 420$ nm)	1962	---	[12]
S-doped g-C_3N_4	300 W Xe lamp ($\lambda \geq 420$ nm)	1148	---	[13]

Carbon defective g-C_3N_4	300 W Xe lamp ($\lambda \geq 420$ nm)	1534	2.87%	[14]
B-doped g-C_3N_4	300 W Xe lamp ($\lambda \geq 420$ nm)	1639.3	---	[15]
C- and N-vacancies in g-C_3N_4	300 W Xe lamp ($\lambda \geq 420$ nm)	400	7.6%	[16]
Nitrogen-deficient g-C_3N_4	300 W Xe lamp ($\lambda \geq 420$ nm)	1664	1.25%	[17]
F-doped g-C_3N_4	300 W Xe lamp ($\lambda \geq 420$ nm)	83.89	0.016%	[18]
S, P, O-doped gC_3N_4	300 W Xe lamp ($\lambda \geq 420$ nm)	2480	---	[19]
C-doped gC_3N_4	300 W Xe lamp ($\lambda \geq 420$ nm)	5643	1.41%	[20]
C, O-doped g-C_3N_4 with N_v	**150 W Xe lamp ($\lambda \geq 420$ nm)**	**1850**	**7.1%**	**Present work**

---

*The H_2 evolution rates are listed for reference but are not directly comparable due to variations in experimental conditions, particularly light source intensity. Apparent Quantum Efficiency (AQE) is the recommended metric for comparison in the present study.

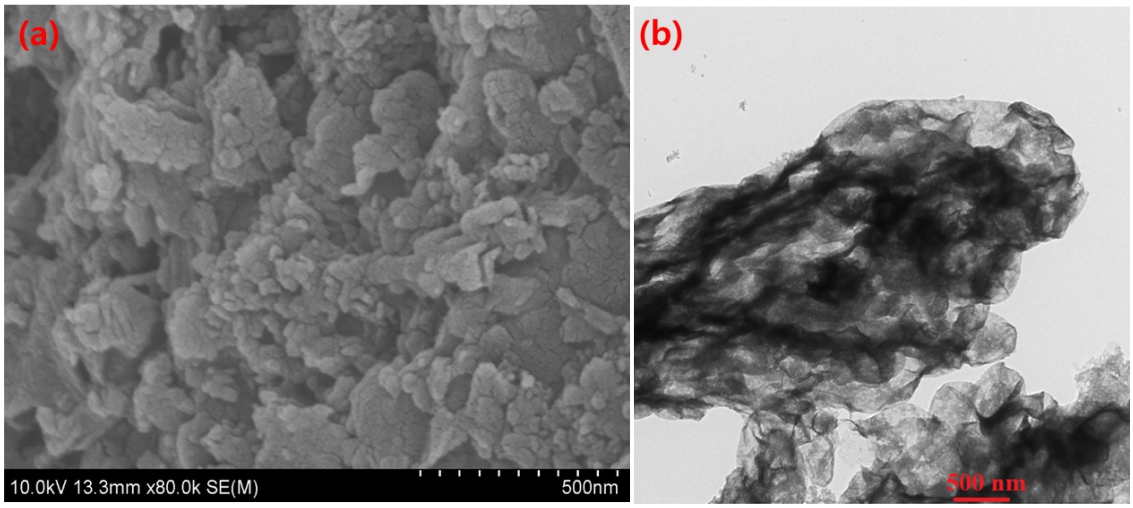

Figure S6. (a) FE-SEM and (b) TEM images of g-C_3N_4 (CN-U) derived from urea precursor

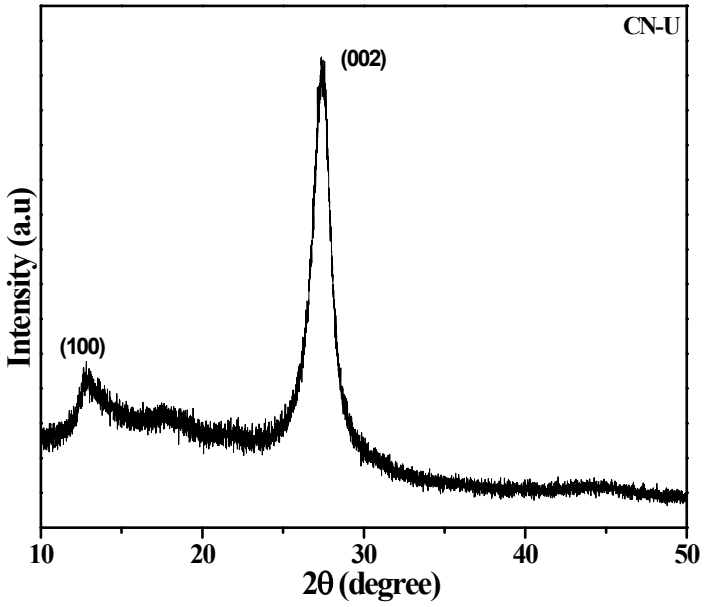

Figure S7. Powder XRD patterns of g-C_3N_4 (CN-U) derived from urea precursor

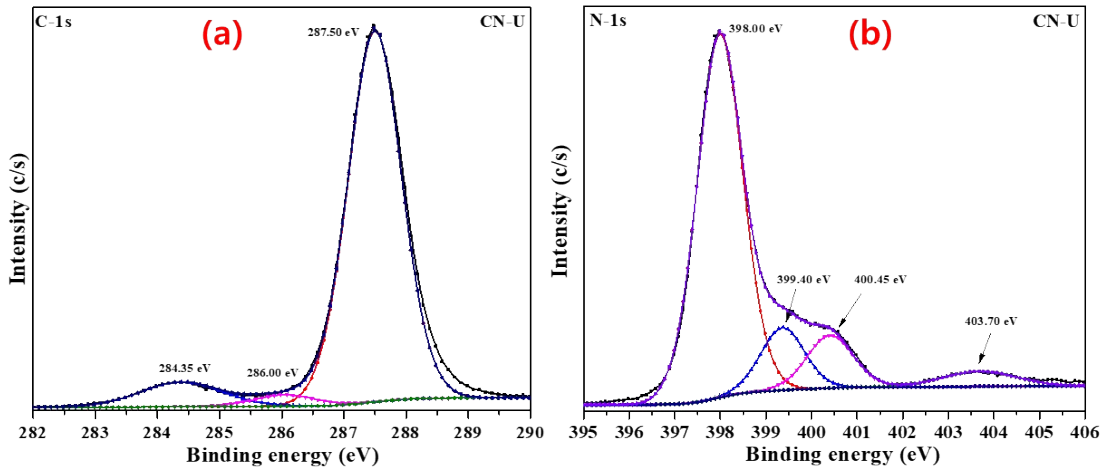

Figure S8. High resolution XPS spectra of (a) C-1s and (b) N-1s in CN-U sample

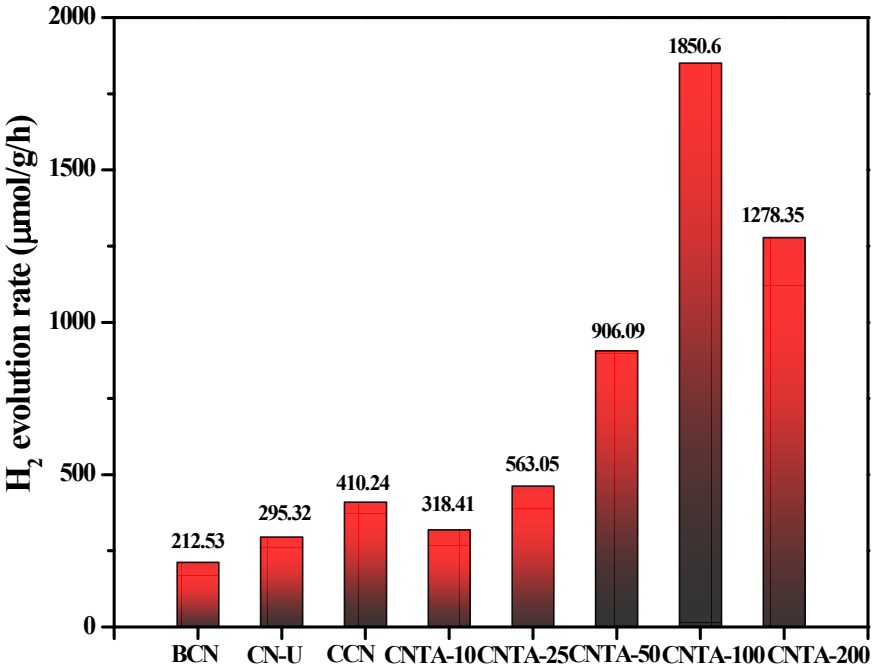

Figure S9. Photocatalytic H_2 evolution activity of BCN, CN-U, CCN and CNTA samples.

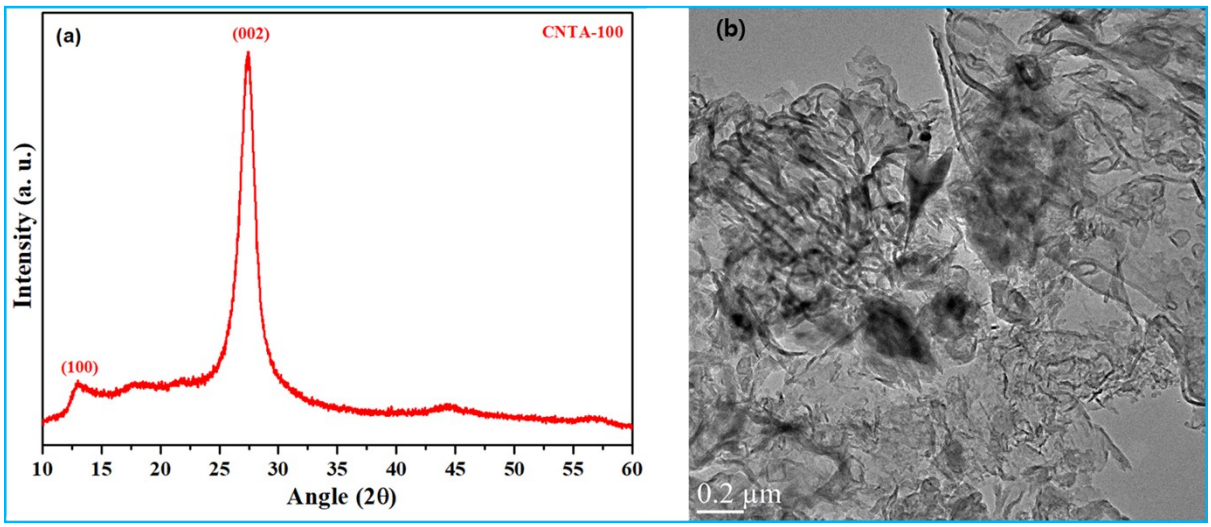

Fig. S10. Powder X-ray diffraction patterns and TEM image of the CNTA-100 photocatalyst sample after cycling experiments of photocatalytic TC degradation reaction.

Table S5. Parameters derived from the fitting of decay profile of BCN and CNTA-100 photocatalyst samples using a bi-exponential fitting decay equation.

sample	τ_1(ns)	A_1(%)	τ_2(ns)	A_2(%)	τ_{avg}
BCN	3.9	4	94	0.0516	18
CNTA-100	3.6	4.2	91	0.0463	16

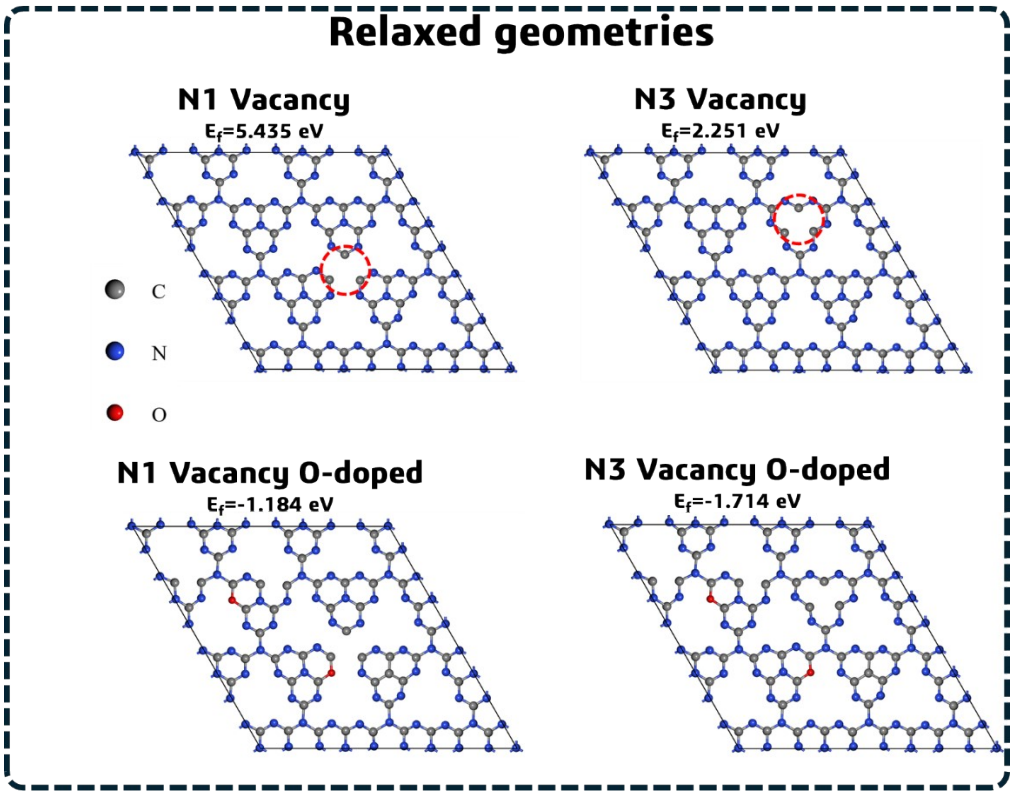

Fig. S11 Optimized atomic configurations of defective (N1 and N2) and oxygen-stabilized g-C_3N_4 (N14 and N2) derived from DFT computations. representative nitrogen vacancy sites (shown by red dashed circles), demonstrating various local coordination settings within the heptazine framework. E_f indicates the formation energy of the N vacancy and O-doping.

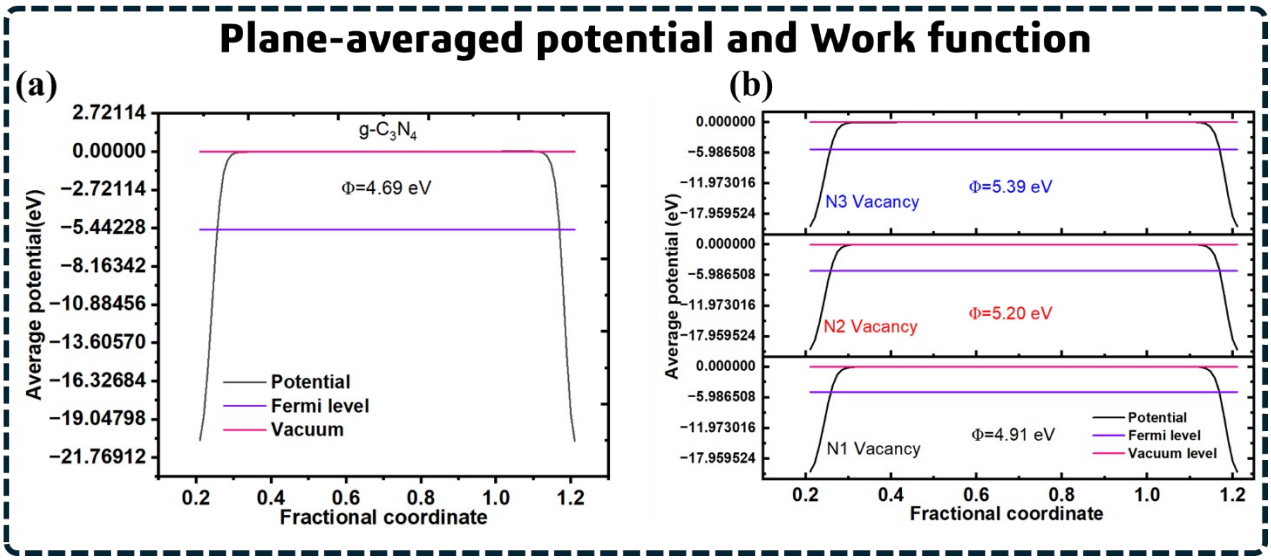

Fig. S12 Planar-averaged electrostatic potential profiles utilized to determine the work function of g-C_3N_4 and nitrogen-vacancy-containing structures. (a) Pristine g-C_3N_4 has a work function of 4.69 eV, derived from the energy disparity between the vacuum level and the Fermi level. (b) Work-function estimates for g-C_3N_4 with nitrogen vacancies N1, N2, and N3, demonstrating vacancy-induced alterations in the surface electronic potential.

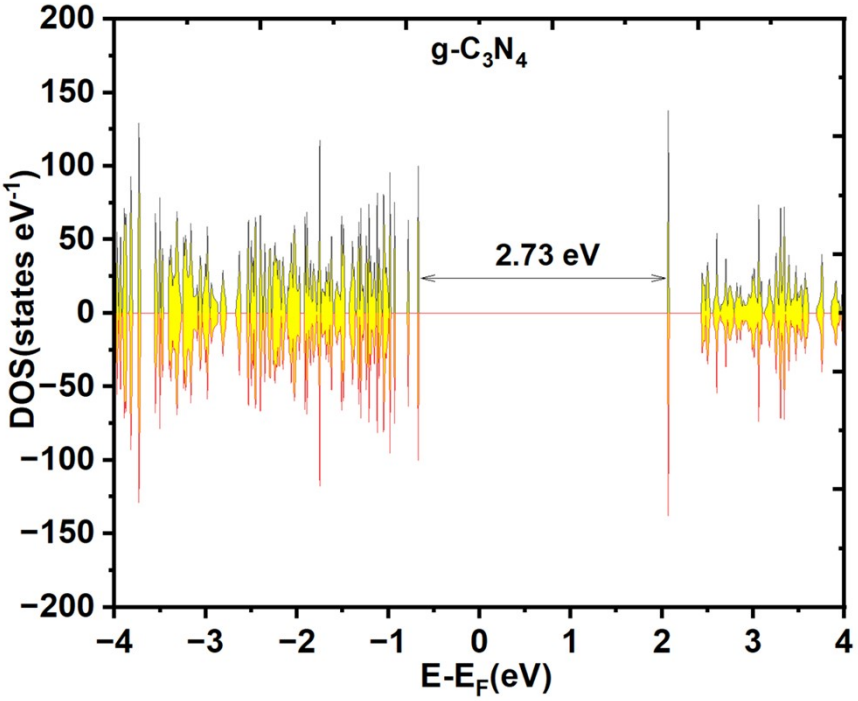

Fig. S13 Total density of states (TDOS) of pristine g-C_3N_4 calculated using density functional theory. The Fermi level is set to 0 eV in order to distinguish the conductance band minimum (CBM) and valence band maximum (VBM). Pristine g-C_3N_4 exhibits a clear semiconducting behavior with an electronic bandgap of **2.73 eV**, consistent with its intrinsic electronic structure and limited visible-light absorption.

References

[1] Yu Zhang, Jingde Luan, Panpan Li, Longde Jiang, Haibin Yan, Wengang Liu, *et al.,* Carbon doping and bridging oxygen benefit for g-C_3N_4 to photocatalytic H_2 production from methanol/water splitting: Experiments and theoretical calculations, Carbon 228 (2024) 119430.

[2] X. –J. Lu, L. Xu, I. Ullah, H. –B. Li, A. –W. Xu, Sulfur-doped g-C_3N_4 photocatalyst for significantly steered visible light photocatalytic H_2 evolution from water splitting, Catal. Sci. Technol. 14 (2024) 606-614.

[3] Zhili Xu, Jing Li, Deyi Zhan, Yue Liu, Weihong Xu, Junfeng Wang, Zhiwu Yu, The n–π* electronic transition induced by nitrogen vacancies enhances, photocatalytic hydrogen production in carbon nitride, Chem. Eng. J. 501 (2024) 157670.

[4] Yabin Jiang, Shaofan Fang, Chi Cao, Enna Hong, Lei Zeng, Wensheng Yang, Limin Huang, Chunzhen Yang, Enhanced light harvesting and charge separation of carbon and oxygen co-doped carbon nitride as excellent photocatalyst for hydrogen evolution reaction, J. Colloids Interface Sci. 2022, 612, 367-376.

[5] Jun Hu, Hongyin Liu, Chun Sun, Lixu Wu, and Feipeng Jiao, Precise Defect Engineering with Ultrathin Porous Frameworks on g-C_3N_4 for Synergetic Boosted Photocatalytic Hydrogen Evolution, Ind. Eng. Chem. Res. 63 (2024) 2665−2675.

[6] Yanping Liu, Wen Yin, Qingyun Lin, Zhigang Li, Wenwu Zhong, Baizeng Fang, Nitrogen vacancies-engineered graphitic carbon nitride nanosheets for boosting photocatalytic H_2 production, Applied Surface Science 640 (2023) 158386.

[7] Bin Wang, Hairui Cai, Daming Zhao, Miao Song, Penghui Guo, Shaohua Shen, Dongsheng Li, Shengchun Yang, Enhanced photocatalytic hydrogen evolution by partially replaced corner-site C atom with P in g-C_3N_4, Applied Catalysis B: Environmental 244 (2019) 486–493.

[8] Zhili Xu, Jing Li, Deyi Zhan, Yue Liu, Weihong Xu, Junfeng Wang, Zhiwu Yu, The n–π* electronic transition induced by nitrogen vacancies enhances photocatalytic hydrogen production in carbon nitride, Chemical Engineering Journal 501 (2024) 157670.

[9] Yongkang Quan, Ruidong Li, Xingzhou Li, Rongxing Chen, Yun Hau Ng, Jianying Huang, Jun Hu, Yuekun Lai, S-modified Graphitic Carbon Nitride With Double Defect Sites For Efficient Photocatalytic Hydrogen Evolution, Small 2024, 20, 2406576

[10] Yaxi Tian, Danni Zeng, Tingzhe Shen, Rongfeng Guan, Wenyan Shi, One-step synthesis of S-doped C-vacancy g-C_3N_4 with honeycomb porous nanosheets structure for efficient visible-light-driven hydrogen evolution, Fuel 357 (2024) 129927.

[11] Chun-Feng Li, Yong-Fei Ji, Qiu-Yu Wei, Zhen-Bang Liu, Yun-Yun Wu, Li−Si Chen, Dong-Xue Han, Li Niu, Chun-Lan Tao, Dong-Dong Qin, Defect and Electronic Structure Engineering Graphitic Carbon Nitride with Dual-Gas-Phase Reaction for Visible-Light-Driven Hydrogen Evolution, ACS APpl. Energy Mater. 2023, 6, 997-1007.

[12] Hao Chen, Wuyou Wang, Zhenzhen Yang, Xian Suo, Ziyang Lu, Weiming Xiao and Sheng Dai, Alkaline salt-promoted construction of hydrophilic and nitrogen deficient graphitic carbon nitride with highly improved photocatalytic efficiency, J. Mater. Chem. A 2021, 9, 4700-4706

[13] Yongkang Quan, Jianna Li, Xingzhou Li, Rongxing Chen, Yingzhen Zhang, Jianying Huang, Jun Hu, Yuekun Lai, Molten salt-assisted synthesis of carbon nitride with defective sites as visible-light photocatalyst for highly efficient hydrogen evolution, Applied Catalysis B: Environment and Energy 362 (2025) 124711

[14] Bin Yang, Jun Han, Qian Zhang, Guangfu Liao, Wenjin Cheng, Guixian Ge, Jichang Liu, Xiaodong Yang, Rongjie Wang, Xin Jia, Carbon defective g-C_3N_4 thin-wall tubes for drastic improvement of photocatalytic H_2 production, Carbon 2023, 202,348-357.

[15] Xiang Xia, Cong Xie, Baogang Xu, Xingshuai Ji, Guanggang Gao, Ping Yang, Role of B-doping in g-C_3N_4 nanosheets for enhanced photocatalytic NO removal and H_2 generation, J. Ind. Eng. Chem. 2022, 105, 303-312.

[16] Lee-Lee Chang, Chechia Hu, Chun-Yao Wang, Wen-Ling Chen, Kanta Yamada, An-Yu Wu, Masaaki Yoshida, Szu-Chia Chien, Kuo-Lun Tung, Synergistic effects of carbon and nitrogen vacancies in carbon nitride for photocatalytic H_2 production and tetracycline oxidation, Separation Purification Tech. 2025, 354, 129346.

[17] Linjie Fan, Yixun Cao, Yushuai Jia, Ruolan Zhu, Deji Zhang, Xin Liu, Surface nitrogen defect modified crystalline carbon nitride spheres with boosted carrier dynamics for efficient solar hydrogen production, Separation Purification Tech. 2025, 354, 129254.

[18] Ji Wu1, Zhonghuan Liu, Xinyu Lin, Enhui Jiang, Shuai Zhang, Pengwei Huo, Yan Yan, Peng Zhou, Yongsheng Yan, Breaking through water-splitting bottlenecks over carbon nitride with fluorination, Nat. Commun. 2022, 13, 6999.

[19] Qinqin Liua, Jiyou Shena, Xiaohui Yua, Xiaofei Yangb, Wei Liua, Juan Yanga, Hua Tang, Hui Xu, Huaming Li, Youyong Li, Jingsan Xu, Unveiling the origin of boosted photocatalytic hydrogen evolution in simultaneously (S, P, O)-Codoped and exfoliated ultrathin g-C_3N_4 nanosheets, Appl. Catal. B., 2019, 248, 84–94.

[20] Hao Yuan, Haoran Sun, Yuxing Shi, Jiaxuan Wang, Ang Bian, Youyou Hu, Feng Guo, Weilong Shi, Xin Du, Zhenhui Kang, Cooperation of carbon doping and carbon loading boosts photocatalytic activity by the optimum photo-induced electron trapping and interfacial charge transfer, Chem. Eng. J. 2023, 472, 144654.